# Open FOAM simulations of the supersonic flow around cones at angles of attack

## Denis Lorenzon[1,2], Sergio Elaskar[1,2]

*[1](Departamento de Aeronautica, Facultad de Ciencias Exactas, Fisicas y Naturales, Universidad Nacional de Cordoba, 5000 Cordoba, Argentina*
*[2](Instituto de Estudios Avanzados en Ingenieria y Tecnologia (IDIT), CONICET - Universidad Nacional de Cordoba, 5000 Cordoba, Argentina*
*Corresponding Author: Denis Lorenzon*

**Abstract:** *The supersonic flow around conical bodies is a very important issue in aerospace engineering, with many applications in internal and external supersonic aerodynamics. Non-viscous supersonic flow about yawing cones is essentially 3-dimensional, but it shows some characteristics regarding the conical flow around circular cones with zero angle of attack. In this latter case, the complete flow structure is axisymmetric and can be described by an ordinary differential equation known as the Taylor-Maccoll equation. When the angle of attack is non-zero, the flow is still conical, i.e., the properties are constant over straight lines passing through the vertex (they are independent of the radial coordinate $r$, even though they depend on the polar $\theta$ and azimuthal $\varphi$ coordinates. This kind of flow has the following remarkable characteristics: a) the shock wave angle depends on the meridian angle, i.e., $\sigma = \sigma(\varphi)$, b) the streamlines between the shock and the cone surface are curved in three dimensions, c) the flow between the cone and the shock wave exhibits entropic gradients perpendicular to the streamlines which makes it rotational, d) in the vertical plane, there exists a radial line on which converge streamlines with different entropy, called vorticity singularity. If the angle of attack is smaller or larger than the cone's half-angle, this vorticity singularity will be attached to the upper surface of the body or separated above it, respectively, e) as the relation between the angle of attack and the aperture angle increases, the cross flow velocity can become supersonic and embedded (or internal) shock waves may appear. Experimental measurements show that the windward flow is accurately described by the non-viscous analysis, however the leeward region is characterized by flow separation. Associated with this flow separation there come up primary and secondary vortices, and if the cross flow velocity is supersonic, two pairs of internal shock waves will appear produced by the sudden change in the flow direction in the separation zone. In this paper we analyze the abilities of the rhoCentralFoam solver of the OpenFOAM suite for the numerical simulation of these flows, using a grid which is coarse enough to be run in a desktop computer. The main objective is to describe the 3D features of the supersonic flow around yawing cones using a modern software, like OpenFOAM, without the need for a computing cluster.*
*Keywords: OpenFOAM, Supersonic flow, Yawing cones, Embedded shock waves, Vortex singularity.*

## I. Introduction

The supersonic conical flow is a very important issue in aerospace engineering, it has several applications in supersonic internal and external aerodynamics. The determination of the properties of high velocity flows around circular cones with an angle of attack has been the subject of numerous theoretical and experimental investigations even before the rise of supersonic flight. (Tracy, 1963) was the first to perform extensive measurements on the flow around cones and try to describe the structure of the flow on the downstream side. Feldhuhn et al. (Feldhuhn, 1969, 1971) provided an accurate empirical description of the flow in the leeward region of cones with high attack angles at supersonic speeds. After that, several experimental studies were carried out using cones of different opening angles in a wide range of angles of attack (George, 1969, Yahalom, 1971). Numerical calculations of the fields of motion in the windward region of cones with a large attack angle were first developed by Moretti (1967), Jones (1969), Kutler (1971), and Fletcher (1975).

Non-viscous supersonic flow around cones with angle of attack is a 3-dimensional phenomenon. However, it has some characteristics of the conical flow around circular cones with zero angle of attack (where the flow is axisymmetric). An ordinary differential equation, the Taylor-Maccoll equation, describes this axisymmetric flow (Taylor and Maccoll, 1933a, 1933b). When the angle of attack of the cone is non-zero, the

flow is still conical, i.e., the properties are constant over straight lines passing through the vertex and depend on the polar $\theta$ and azimuthal $\varphi$ coordinates, but they are independent of the radial coordinate $r$.

This kind of flow has the following remarkable characteristics (see Fig. 1):

a)  the shock wave angle depends on the meridian angle, i.e., $\theta_s = \theta_s(\varphi)$,
b)  the streamlines between the shock and the cone surface are curved in three dimensions,
c)  the flow between the cone and the shock wave exhibits entropic gradients perpendicular to the streamlines which makes it rotational,
d)  in the vertical plane of symmetry, there exists a radial line on which converge streamlines with different entropy, called vorticity singularity. If the angle of attack is smaller or larger than the cone's half-angle, this vorticity singularity will be attached to the upper surface of the body or separated above it, respectively,
e)  as the relation between the angle of attack and the aperture angle increases, the cross flow velocity can become supersonic and embedded (or internal) shock waves may appear. Experimental measurements show that the windward flow is accurately described by the non-viscous analysis, however the leeward region is characterized by flow separation. Associated with this flow separation there come up primary and secondary vortices, and if the cross flow velocity is supersonic, two pairs of internal shock waves will appear produced by the sudden change in the flow direction in the separation zone.

In this paper we analyze the capabilities of the rhoCentralFoam solver of the OpenFOAM suite (https://openfoam.org) for the numerical simulation of these flows, using a grid which is coarse enough to run in a desktop computer. The main objective is to describe the 3D features of the supersonic flow around yawing cones using the OpenFOAM software without the need for a computing cluster. Note that OpenFOAM has been already successfully implemented for supersonic flow in other applications (Lorenzon, 2015, Gutierrez, 2016, 2017a, 2017b, 2019). However, in this work we emphasize the OpenFOAM flexibility to simulate all the features of the conical flow around cones with angle of attack in a personal computer.
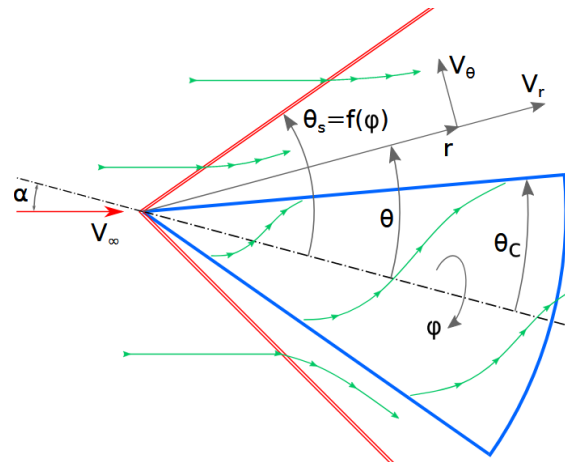


**Fig. 1:** Geometrical description of supersonic conical flow and nomenclature.

## II.  Physical model and numerical scheme

In this section, the fundamental equations and the employed numerical method are briefly introduced.

**Fundamental equations**

To simulate the non-viscous supersonic flow, the Euler equations are considered:

$$\frac{\partial u}{\partial t} + \frac{\partial F_c}{\partial x} = 0$$

where $u$ is the vector of conservative variables:

$$u = (\rho, \rho U_1, \rho U_2, \rho U_3, \rho E)$$

and $F_c$ is the flux vector:

$$F_c = \begin{bmatrix} \rho V_c \\ \rho U_1 V_c + n_1 p \\ \rho U_2 V_c + n_2 p \\ \rho U_3 V_c + n_3 p \\ (\rho E + p) V_c \end{bmatrix}$$

where $U$ is the velocity vector, $\rho$ the density, $p$ the pressure, $E$ the total energy, and $V_c = U \cdot \vec{n}$ the contravariant velocity (Hung, 2002). The total energy $E$ for a perfect gas is:

$$E = \int_{T_0}^{T} c_v dT - R T_0 + \frac{1}{2} U^2$$

where $R$ is the gas constant and $c_v$ the specific heat for constant volume. Finally, the equation of state for perfect gases is used, $p = \rho R T$ .

**Finite volume formulation**

Mass, momentum and energy conservation equations are solved using the finite volume method. In this method, the physical domain is discretized in small volumes or cells as shown in Fig. 2. There are internal faces between the proprietary ( $P$ ) and the neighbor ( $N$ ) cells. In this paper, a cell-centered formulation is implemented; therefore, all the thermo-physical properties and the flow variables are stored in each cell centroid (e.g. $P$ in Fig. 2). The face vector $S_f$ points outwards from the inner surface, the vector $d_{PN}$ goes from the centroid of cell $P$ to that of neighboring cell $N$ , and the vector $d_{fN}$ joins the centroid of cell $N$ with the center of the inner face.
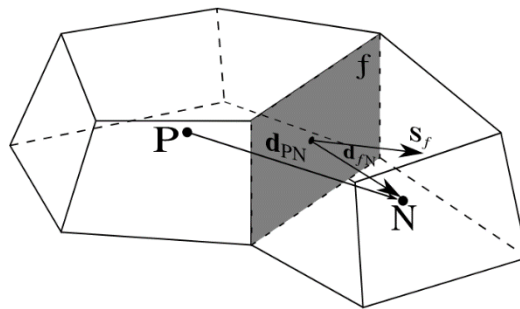


**Fig. 2:** Physical domain discretization with finite volumes ( $N$ : neighbor cell, $P$ : proprietary cell, $d_{PN}$ : vector between the proprietary and neighbor cells, $d_{fN}$ : vector between the centroid of the face and that of the neighboring cell, $S_f$ : surface vector of the face (normal vector to the face whose magnitude is the area of that face).

## III. Mesh, boundary and initial conditions

When the cone moves relative to the air with zero angle of attack, all the flow variables are independent from both $r$ and $\varphi$ , which allows to simulate the conical flow using bi-dimensional domains. On the other hand, when the angle of attack is non-zero, there is just one symmetry plane and the domain needs to be 3-dimensional. All 3D meshes used in this work were generated using the blockMesh utility included in the OpenFOAM suite. They are composed by four blocks of hexahedral cells totaling $1710720$ cells. In Fig. 3 it is shown the geometrical domain and the nomenclature set for the patches at each boundary. Tables 1 shows the imposed boundary conditions to each patch, where the initial conditions set within the domain are designated by internalField. Figure 4 illustrates the employed meshes with a schematic resolution.
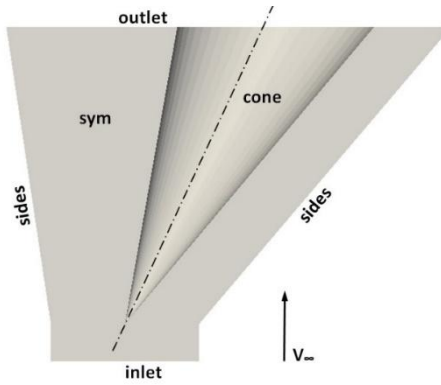
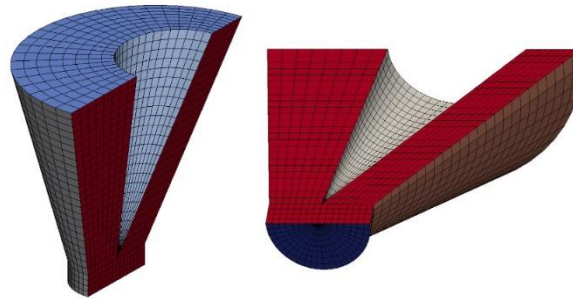**Fig. 3:** Geometrical domain and patches nomenclature.



**Fig. 4:** Structured mesh generated with blockMesh (schematic resolution).

**Table 1:** Boundary and initial conditions.

|  | P [Pa] | T [K] | **U** [m/s] |
|---|---|---|---|
| inlet | 101325 | 288.15 | $(U_1, 0, 0)$ |
| outlet | zeroGradient | zeroGradient | zeroGradient |
| sides | 101325 | 288.15 | $(U_1, 0, 0)$ |
| cone | zeroGradient | zeroGradient | slip |
| sym | symmetryPlane | symmetryPlane | symmetryPlane |
| internalField | 101325 | 288.15 | $(U_1, 0, 0)$ |

## IV. Results

To validate the numerical results, the simulated test cases are the corresponding to those experimentally studied by Yahalom (1971). The free stream Mach number is $M_1 = 2.72$, the cones aperture angles are $\theta_c = 10°$, $15°$, and $20°$, and the angle of attack is varied from $\alpha = 5°$ to $30°$ with increments of $5°$. The experimental investigations of Yahalom (1971) were performed at the Aeronautical Sciences Division of the California University in Berkeley. In these tests, the ambient thermodynamic conditions were: stagnation pressure $P_0 = 60.33\,kPa$, stagnation temperature $T_0 = 294.3\,K$ and Reynolds number $\Re = 5450000/m$.

To compare our simulation results with the experimental data, we use the distribution of circumferential static pressures over the cone surface, the aerodynamic forces coefficients, the shape of the external shock wave, the position of the internal shock waves, the stagnation points in the cross flow plane, and the flow field properties at the meridian plane ($\varphi = 180°$).

**Pressure distribution**
To describe the circumferential pressure distribution, we calculate the pressure coefficient as

$$C_p = \frac{p_c - p_\infty}{\frac{1}{2}\gamma\, p_\infty M^2}$$

where $p_c$ is the pressure on the cone surface, $p_\infty$ is the pressure of the unperturbed stream, and $\gamma$ is the adiabatic coefficient or ratio of specific heats.

Figures 5 to 7 compare the numerical and experimental distributions of $C_p$ on the cone surface for different angles of attack. The continuous curves are the simulation results, while the discontinuous ones represent the experimental data from Yahalom (1971). Figures 5, 6 and 7 correspond to the cones with angles of $10°$, $15°$ and $20°$, respectively.

From the figures, we can observe that as the angle of attack increases, the $C_p$ increases rapidly in the windward side and decreases moderately in the opposite side (leeward). When $\alpha$ is small relative to the cone angle ( $\alpha/\theta_c < 2/3$ ), the pressure decreases monotonously with $\varphi$ reaching its minimum value at $\varphi = 180°$. For larger relative incidences up to $\alpha = \theta_c$, the point of minimum pressure moves away from the symmetry plane to $\varphi$ between $120°$ and $150°$. In this case, the behavior observed in the experimental data is not clearly captured by the numerical simulations. The numerical results show a very good accuracy in comparison with the experimental data when the angle of attack is smaller than the cone angle.

When $\alpha/\theta_c > 1$ the differences become significant. In the numerical simulations the pressure decreases monotonously up to a local minimum between $\varphi = 130°$ and $150°$, after which a sudden low intensity compression happens. Then, the pressure increases smoothly until $\varphi = 180°$. This pressure jump is due to the primary embedded shock waves and, as the angle of attack becomes higher, it gets stronger and closer to the symmetry plane. On the other hand, the experimental data suggests that $\alpha$ does not affect the location of the minimum $C_p$ point, after which the pressure maintains approximately constant.

It is possible to attribute the difference in the pressure behavior in the leeward side to viscous effects, since the flow in this region is characterized by the boundary layer detachment and vortices formation. Nevertheless, the simulation results presented here are similar to other numerical computations based on non-viscous models, such as that from Kutler (1971). Rainbird (Rainbird, 1968a, 1968b), carried out experimental measurements of the circumferential pressure around a $5°$ cone with relative angles of attack of $2.1$ and $2.5$, and Mach numbers of $1.79$ and $4.25$. His results indicate that in the leeward side there are two local pressure minima. The first one is notably more pronounced and is followed by an abrupt pressure increase similar to those observed in the simulations shown here.
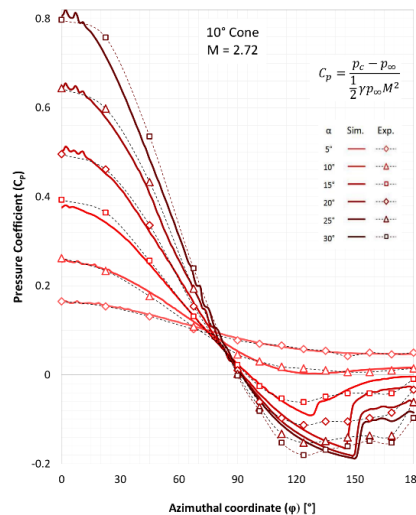


**Fig. 5:** Circumferential pressure distribution for the 10° cone. Sim.: Numerical results obtained with rhoCentralFoam. Exp.: Experimental results of Yahalom (1971).
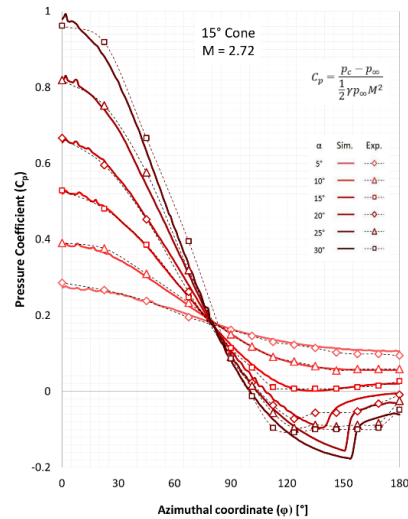
**Fig. 6:** Circumferential pressure distribution for the 15° cone. Sim.: Numerical results obtained with rhoCentralFoam. Exp.: Experimental results of Yahalom (1971).
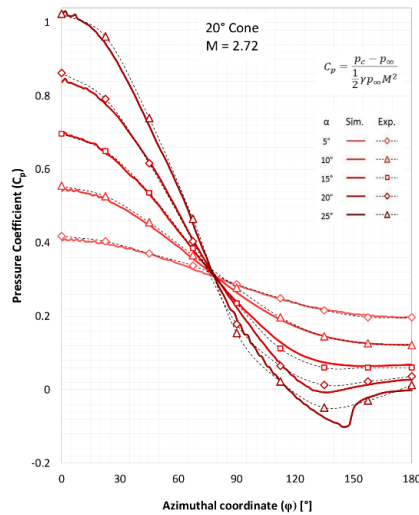


**Fig. 7:** Circumferential pressure distribution for the 20° cone. Sim.: Numerical results obtained with rhoCentralFoam. Exp.: Experimental results of Yahalom (1971).

**Coefficients of static forces**

Integrating numerically the distribution of pressure coefficients, the axial and normal forces coefficients $C_A$ and $C_N$ are calculated as:

$$C_A = \frac{1}{\pi} \int_0^\pi C_p(\varphi)\, d\varphi$$

$$C_N = \frac{1}{\pi \tan \theta_c} \int_0^\pi C_p(\varphi) \cos \varphi \, d\varphi$$

Once the coefficients $C_A$ and $C_N$ have been determined, the drag and lift coefficients $C_D$ and $C_L$ can be evaluated as follows:

$$C_D = C_A \cos \alpha + C_N \sin \alpha$$
$$C_L = C_N \cos \alpha - C_A \sin \alpha$$

The obtained drag and lift coefficients are plotted for different relative angles of attack in Figs. 8 and 9, respectively. The blue, green and red curves correspond to the cones with aperture angles of 10°, 15° and 20°, respectively. In the same plots, comparisons are made with the experimental results of Yahalom (1971).

The drag coefficient behavior is similar for all studied cones and it consists of a non-linear increase with the angle of attack. For the same ratio $\alpha/\theta_c$ , the slope $C_{D\alpha}$ is greater the greater the angle of the cone. If $\alpha/\theta_c < 1.5$ , the simulation results show a very good accuracy regarding the experimental values. But for higher angles of attack, the obtained numerical values are slightly lower.

The lift coefficient increases in an approximate linear way with $\alpha/\theta_c$ , except for large relative angles of attack, where $C_L$ grows more slowly $C_{L\alpha}$ starts to decrease). The correlation with the experimental data is again very good for $\alpha/\theta_c < 1.5$ . For higher values, the differences increase, especially for the 10° cone where the slope obtained with the rhoCentralFoam solver is lower and more alike the one given by Sims (1964).
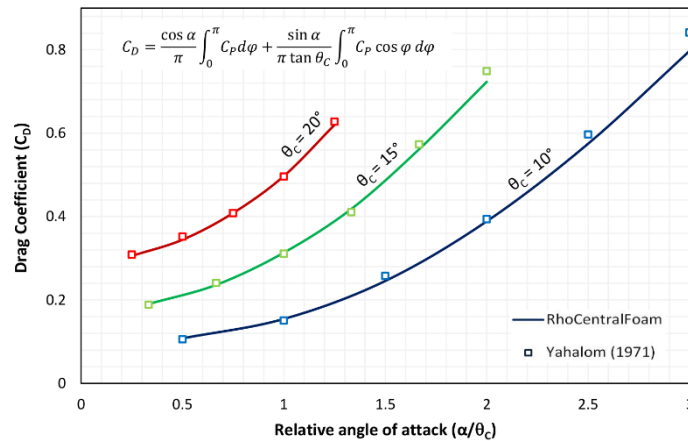


**Fig. 8:** Variation of $C_D$ with $\alpha$ for the different cones. $M = 2.72$ .
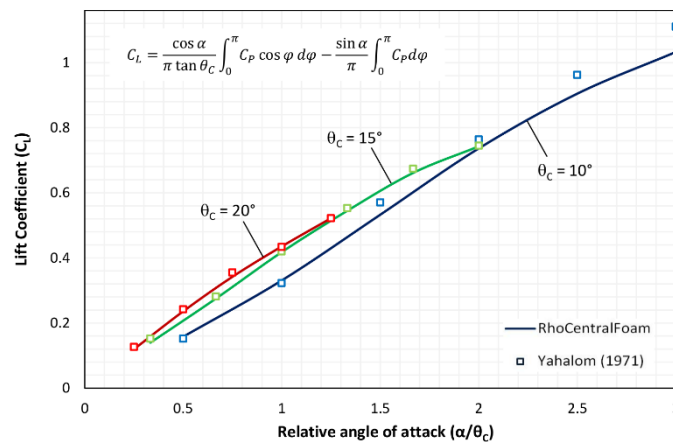


**Fig. 9:** Variation of $C_L$ with $\alpha$ for the different cones. $M = 2.72$ .

**External shock wave**

The external shock wave separates the free stream from the flow field perturbed by the cone. Figures 10 - 12 show the shape of the external shock wave projected over a plane perpendicular to the cone axis. The obtained numerical results are shown for different cones and angles of attack, and correspond to the continuous lines. For comparison, the experimental data of Yahalom (1971) is represented by the red points.

From the figures, we can note that for $\alpha < 20°$ there is good agreement between the numerical and experimental data. However, when $\alpha > \theta_c$ the accuracy is not so good. In all cases, as $\alpha$ increases, the external shock wave angle $\theta_s$ remains approximately constant in the incidence side, and the numerical results agree with the experimental ones. On the other hand, in the leeward side, $\theta_s$ is lower than that obtained by Yahalom (1971), although it retains a good accuracy if compared to the numerical results of Jones (1969). Note that the results in this paper does not contain any viscous effects, e.g., boundary layer effects.

We highlight that the shock wave at the leeward side is weak. In fact, it is so weak that cannot be visualized through Schlieren techniques. If $\alpha/\theta_c > 1$ , the pressure increment across the shock for large values

of $\varphi$ is less than $5$ of the unperturbed pressure. As a consequence, it is difficult to determine numerically and experimentally the shock wave position with high accuracy. The variations in density and temperature are even weaker than the pressure ones.
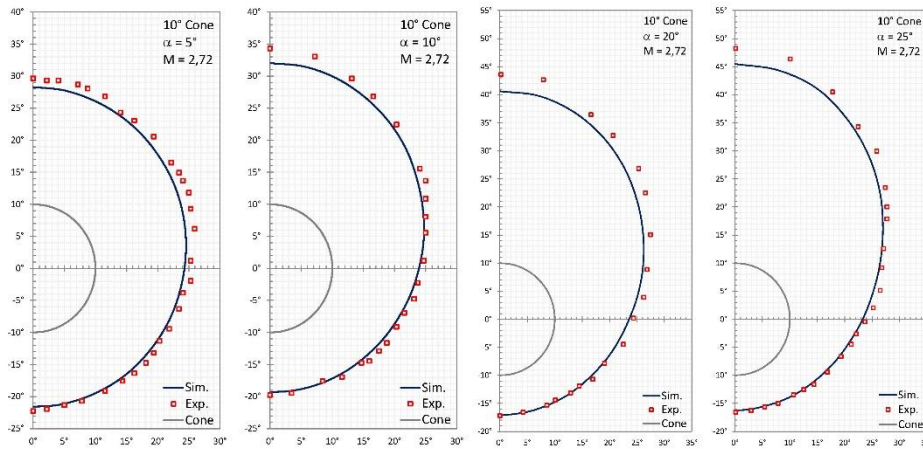


**Fig. 10:** External shock wave for the 10° cone for different $\alpha$ . Sim.: rhoCentralFoam. Exp.: Yahalom (1971).
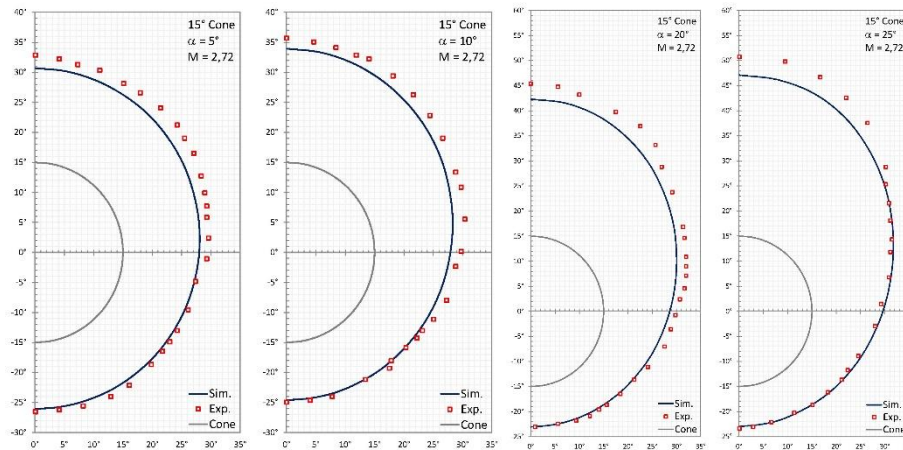


**Fig. 11:** External shock wave for the 15° cone for different $\alpha$ . Sim.: rhoCentralFoam. Exp.: Yahalom (1971).
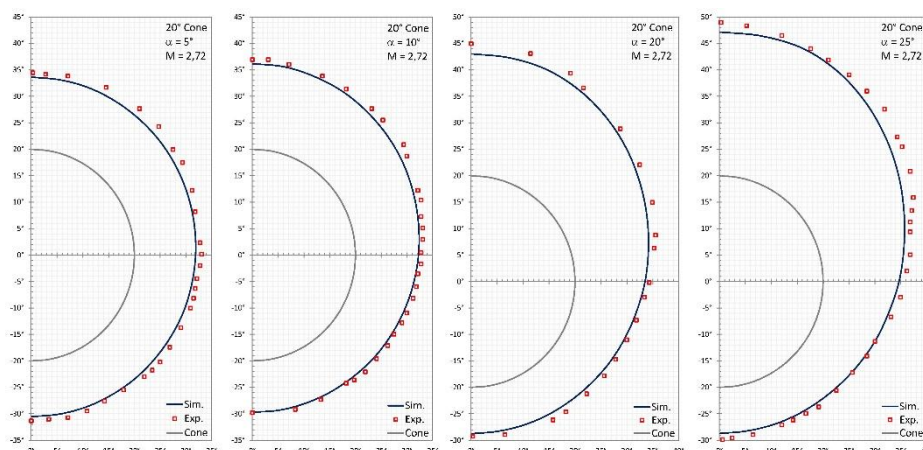


**Fig. 12:** External shock wave for the 20° cone for different $\alpha$ . Sim.: rhoCentralFoam. Exp.: Yahalom (1971).

**Flow in the plane** $\varphi = 180°$

So far, the flow properties on the windward side of the cone were accurately described by the rhoCentralFoam solver. We now study the distribution of the flow variables with the polar coordinate $\theta$ at the symmetry plane on the leeward side. For convenience, we introduce a new variable $\varsigma$ defined as:

$$\xi = \frac{\tan\theta - \tan\theta_c}{\tan\theta_s - \tan\theta_c}$$

which varies from $0$ at the cone surface to $1$ at the shock wave. The pressure distribution is shown in Figs. 13 - 15, and the temperature distribution in Figs. 16 - 18.

From the figures, we can appreciate that when the angle of attack is smaller than the cone angle there is a small compression from the shock wave to the cone surface. On the contrary, for ratios $\alpha/\theta_c > 1$, the pressure decreases as getting closer to the cone surface. For $\alpha = \theta_c$, it is verified both numerically and empirically that the static pressure is maintained almost constant for all $\xi$. In general, the agreement between the simulation and the results from Yahalom (1971) is very good for small values of $\alpha$, but gets worse for high relative angles of attack. For angles of attack up to the cone angle, the static temperature variation in the symmetry plane is small, and its behavior is similar to that of the static pressure.

The Jones theory (Jones, 1969) exhibits a pronounced temperature gradient near the wall, which has not been detected in the present simulations nor in Yahalom's experiments. For higher relative incidence angles, the temperature decreases slightly in the expansion regions and increases close of the cone surface. For very large ratios $\alpha/\theta_c$, it is observed that the temperature increase is interrupted by a negative gradient close the cone which is followed by a steep increase on the wall. The experimental data agrees with this steep increase in temperature next to the wall but does not capture the negative gradient before it.
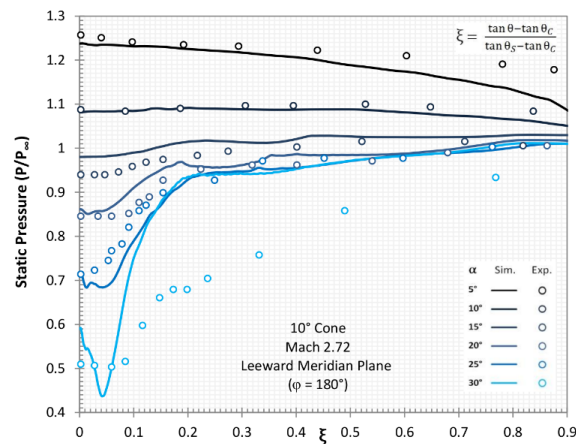


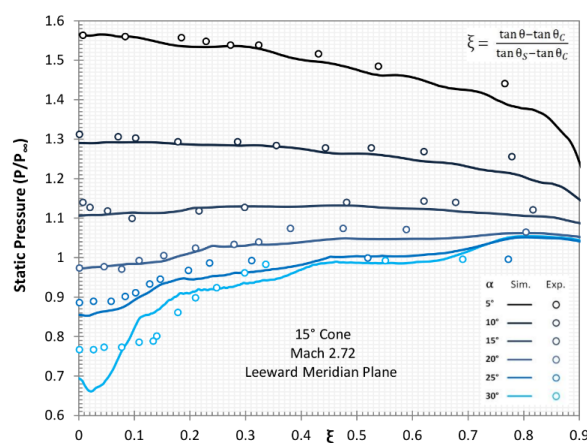**Fig. 13:** Static pressure variation in the plane $\varphi = 180°$. 10° cone.



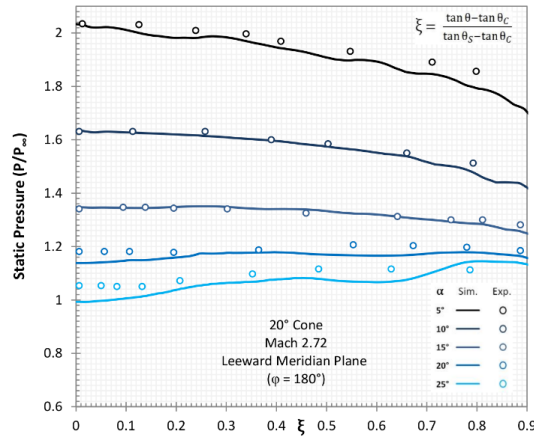**Fig. 14:** Static pressure variation in the plane $\varphi = 180°$. 15° cone.

**Fig. 15:** Static pressure variation in the plane $\varphi = 180°$ . 20° cone.



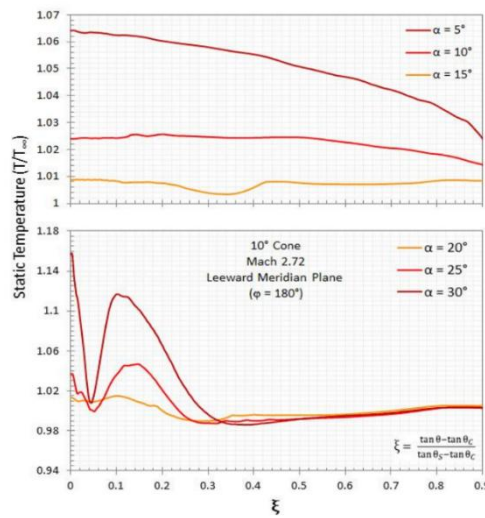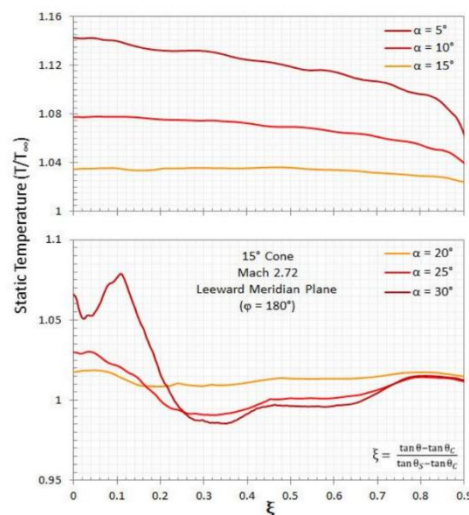**Fig. 16:** Static temperature variation in the plane $\varphi = 180°$ . 10° cone.



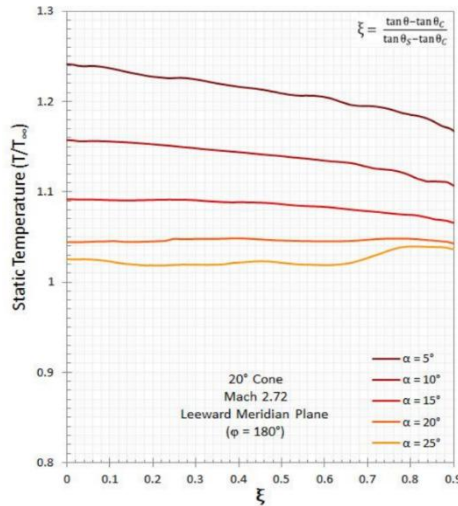**Fig. 17:** Static temperature variation in the plane $\varphi = 180°$ . 15° cone.

**Fig. 18:** Static temperature variation in the plane $\varphi = 180°$. 20° cone.

**Embedded shock waves**

The embedded or internal shocks appear inside the region perturbed by the cone (i.e. between the external shock wave and the cone surface). These discontinuities emerge when the angle of attack exceeds considerably the cone angle, and their extension and intensity are relatively small. The theory of non-viscous flow around circular cones predicts the appearance of these waves when the cross-flow velocity is supersonic. In experimental studies, it is observed that they appear close to the primary points of separation of the boundary layer, and for relative incidences higher than $1.3$.

In all our numerical tests verifying $\alpha/\theta_c > 1$, internal shocks were captured. For higher relative angles of attack, the internal shocks not only grow in size and intensity, but also a new pair of shock waves are formed normal to the symmetry plane. These are known as secondary embedded shock waves. Both pairs of internal shocks were first noted experimentally by Tracy (1963) and Feldhuhn (1970), despite being difficult to detect through Schlieren techniques because of their weakness.

The internal shock waves can be seen in Figs. 19 and 20 for the 10° and 15° cones, respectively. These figures show the numerical pressure field projected on a plane perpendicular to the longitudinal axis of the cone together with Yahalom empirical estimations about the position of the internal shocks. The numerical results regarding the external shock show a good agreement with the experimental data, however, the numerical internal shocks ($S-S$) are placed significantly closer to the symmetry plane that the ones measured experimentally ($E-E$). This difference increases with $\alpha$, and it is probably caused by viscous effects, which are important for the structure of the flow in that region, and are not considered in the physical model for the numerical simulations. Similar appreciations were made by Fletcher (1975).
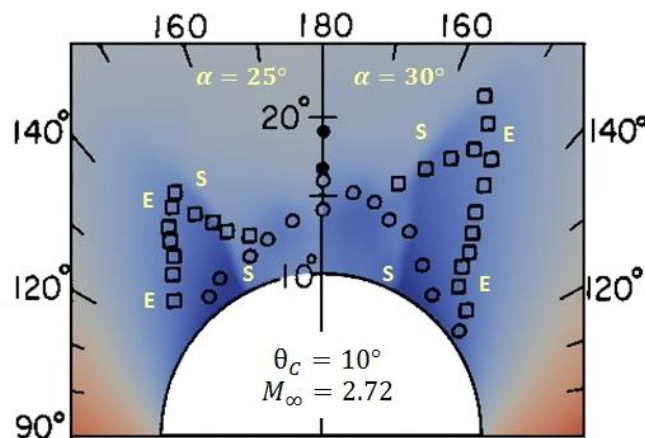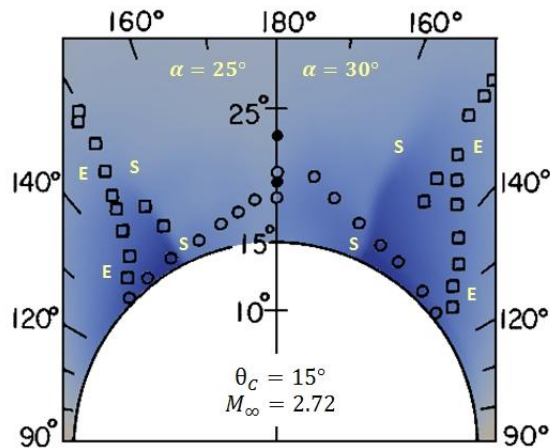


**Fig. 19:** Static pressure field and embedded shock waves. $S-S$: Numerical. $E-E$: Yahalom (1971). 10° cone.

**Fig. 20:** Static pressure field and embedded shock waves. $S-S$ : Numerical. $E-E$ : Yahalom (1971). 15° cone.

**The vortex singularity**

 A very useful way of representing conical flows is through their projection over a spherical surface generated by the points at constant distance from the vertex. When this projection is examined in the direction of the cone axis, it is called cross flow plot or plot on the cross flow plane. The vorticity singularity is a stagnation point in the cross flow plane, which means that the only non-zero component of the velocity is the radial one. This point is characterized by the convergence of streamlines with different entropy, and could be placed on the surface of the cone or at a certain distance above it depending on the angle of attack. From the non-viscous flow theory, if the entropy is not uniquely determined on the vorticity singularity, the same is true for the stagnation pressure.

 If we consider the effects of viscosity, the singularity is a small zone and not a discontinuity. When the singularity is placed near the cone surface, it interacts with the boundary layer or with the detached flow and is difficult to be captured experimentally. To determine the existence of these singular points, Feldhuhn (1969) and George (1969) carried out experiments under different conditions, and they used the zero cross-flow velocity criterion and the jump in stagnation pressure criterion, respectively.

 Yahalom (1971) used the zero cross-flow Mach number $M_\theta$ criterion to identify these singularities. However, this technique was not effective enough due the formation of two other stagnation points in the cross-flow plane. One of them is generated by the formation of two circulation zones at each side of the cone, and the other is located at the intersection of the symmetry plane with the cone surface. Rainbird (1968) estimated that the vorticity singularity only separates from the cone for angles of attack twice the angle of the cone. For larger $\alpha$, from the two stagnation points in the cross-flow plane, the vorticity singularity is the one placed further from the cone. Yahalom noticed, in some cases, a small region where $M_\theta$ is close to zero and assumed that both stagnation points are next to each other, and indistinguishable. The distance between them could grow as the relative incidence increases.

 Figures 21 and 22 show the variation of $M_\theta$ from the cone surface to the external shock wave, obtained in our simulations for small and large relative angles of attack, respectively. From the figures, we see that the case with $\theta_c = 10°$ and $\alpha = 30°$, is the only one where clearly exists cross-flow stagnation points ( $M_\theta = 0$ ) others than $\xi = 0$ .
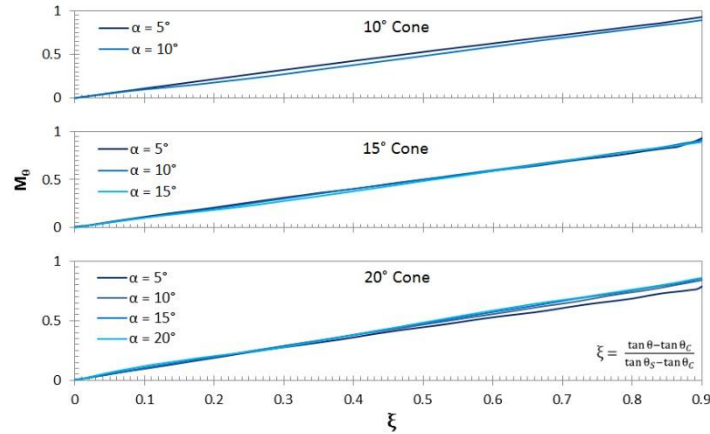
**Fig. 21:** Cross flow Mach number $M_\theta$ in the plane $\varphi = 180°$. Small $\alpha/\theta_c$.



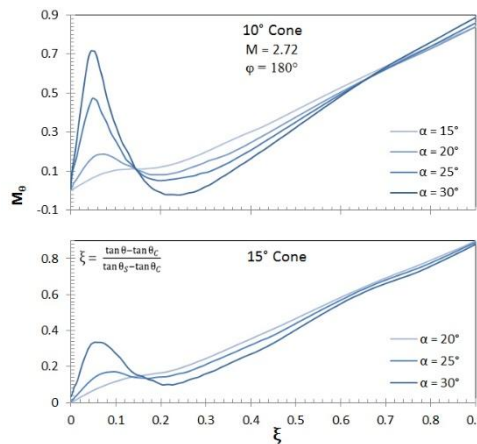**Fig. 21:** Cross flow Mach number $M_\theta$ in the plane $\varphi = 180°$. Large $\alpha/\theta_c$.

## V.  Conclusions

In this paper, a numerical study about the 3D supersonic flow around cones with angles of attack is carried out using the rhoCentralFoam solver of the OpenFOAM suite. This task is developed in order to analyze the capability of this tool to describe accurately the flow properties even when it is implemented in a desktop computer. Therefore, a coarse enough grid is used.

Several tests are performed for different flow parameters. The free stream Mach number is $M_1 = 2.72$, the cones aperture angles are $\theta_c = 10°$, $15°$ and $20°$, and the angle of attack is varied from $\alpha = 5°$ to $30°$ with increments of $5°$. The stagnation temperature and pressure are $T_0 = 294.3\,K$ and $P_0 = 60.33\,kPa$, respectively, and the Reynolds number is $\Re = 5450000/m$. To compare with the experimental data, many parameters are evaluated: the pressure distribution ($C_p$ distribution), the drag and lift coefficients, the external shock wave position, the flow pressure and temperature in the plane $\varphi = 180°$, embedded shock waves, and the vortex singularity.

The numerical results of the $C_p$ distribution for $\alpha/\theta_c < 0.75$ show high accuracy in comparison with the experimental data. For $\alpha/\theta_c > 1$ the discrepancies increase. In the numerical simulation, around $\varphi = 130°$ and $130°$, a sudden low intensity compression happens. This phenomenon does not clearly appear in the experimental data of Yahalom (1971). However, in the experiments developed by Rainbird (1968) there are two local pressure minima. The first one is followed by an abrupt pressure increase similar to those found in the simulations here presented.

The drag and lift coefficients show a very good accordance with Yahalom's data (Yahalom ,1971), mainly for $\alpha/\theta_c < 1.5$. For higher relative attack angles, the numerical values are slightly different. For $\alpha < 20°$, the external shock wave position is accurately captured by the numerical solver. However, when $\alpha > \theta_c$ the accuracy reduces. As the angle of attack increases, the external shock wave angle remains

approximately constant in the incidence side. Whereas at the opposite side (leeward side), numerical $\theta_s$ is lower than the experimental one (Yahalom, 1971), although it is accurate in comparison with the numerical results of Jones (1969).

Both pressure and temperature in the plane $\varphi = 180°$ are accurately calculated by the solver. For $\alpha < \theta_c$ the pressure slightly increases from the shock wave to the surface of the cone. For $\alpha = \theta_c$, the pressure is almost constant for all $\xi$. For $\alpha / \theta_c > 1$, the pressure decreases as getting closer to the cone surface. For $\alpha < \theta_c$ the temperature variation in the symmetry plane is small. For very large ratios $\alpha / \theta_c$, the numerical results show a negative gradient of temperature close the cone which is followed by a steep increase on the wall. The experimental results agree with this steep increase, but do not capture the negative gradient before it.

The numerical simulations capture well the external shock waves, and they show agreement with the experimental results. But the numerical internal shocks are located closer to the symmetry plane than the experimental ones. This difference increases with $\alpha$, and it could be produced by the viscous effects (see Fletcher, 1975). The software can capture the vortex singularity for $\theta_c = 10°$ and $\alpha = 30°$. It is the only studied test with two cross-flow stagnation points ( $M_\theta = 0$ ) apart from $\xi = 0$.

Finally, we highlight that the rhoCentralFoam solver can be used to solve the 3D conical flow for cones with angle of attack in a desktop computer with satisfying results.

## Acknowledgments

## References
[1]. Espinoza, D., V. Casseau, T. Scanlon, and R. Brown (2016). An open-source hybrid CFD-DSMC solver for high speed flows. Victoria, BC, Canada, pp. 050007.
[2]. Falcinelli, O., S. Elaskar, and J. Tamagno (2008, March). Reducing the Numerical Viscosity in Nonstructured Three-Dimensional Finite Volumes Computations. Journal of Spacecraft and Rockets 45(2), 406–408.
[3]. Feldhuhn, R., L. Pasiuk, and A. Winkelmann (1970, June). An experimental investigation of the flow field around a yawed cone. Washington, DC, U.S.A. American Institute of Aeronautics and Astronautics.
[4]. Feldhuhn, R. and A. Winkelmann (1969). Separated Flow Phenomena on a Slender Cone at Mach 5.
[5]. Feldhuhn, R., A. Winkelmann, and L. Pasiuk (1971, June). An Experimental Investigation of the Flowfield around a Yawed Cone. AIAA Journal 9(6), 1074–1081.
[6]. Fletcher, C. (1975, August). Vortical singularity behind a highly yawed cone. AIAA Journal 13(8), 1073 1078.
[7]. George, L. (1969). An Experimental Investigation of the Flow Field Around an Inclined Sharp Cone in Hypersonic Flow. Volume SC-RR-69-577, Sandia Laboratories, Albuquerque, New Mexico.
[8]. Greenshields, C., H. Weller, L. Gasparini, and J. Reese (2009). Implementation of semidiscrete, non-staggered central schemes in a colocated, polyhedral, finite volume framework, for high-speed viscous flows. International Journal for Numerical Methods in Fluids, n/a–n/a.
[9]. Gutierrez Marcantoni, L., J. Tamagno, and S. Elaskar (2016, March). RANS Simulation of Turbulent Diffusive Combustion using Open Foam. Journal of Applied Fluid Mechanics 9(2), 669–682.
[10]. Gutierrez Marcantoni, L., J. Tamagno, and S. Elaskar (2017, October). Twodimensional numerical simulations of detonation cellular structures in H2o2ar mixtures with OpenFOAM. International Journal of Hydrogen Energy 42(41), 26102–26113.
[11]. Gutierrez Marcantoni, L., J. Tamagno, and S. Elaskar (2019, March). A numerical study on the impact of chemical modeling on simulating methane-air detonations. Fuel 240, 289–298.
[12]. Gutierrez Marcantoni, L., J. Tamagno, and S. Elaskar (2017, October). rhoCentralRfFoam: An OpenFOAM solver for high speed chemically active flows Simulation of planar detonations. Computer Physics Communications 219, 209–222.
[13]. Hung, C. (2002, June). Definition of Contravarinat Velocity Components. In 3rd Theoretical Fluid Mechanics Meeting, St. Louis, Missouri. American Institute of Aeronautics and Astronautics.
[14]. Jones, D. (1969). Tables of inviscid supersonic flow about circular cones at incidence, Volume 137 of AGARD. Paris: North Atlantic Treaty Organization, Advisory Group for Aerospace Research and Development.
[15]. Kurganov, A., S. Noelle, and G. Petrova (2001, January). Semidiscrete Central-Upwind Schemes for Hyperbolic Conservation Laws and Hamilton–Jacobi Equations. SIAM Journal on Scientific Computing 23(3), 707–740.
[16]. Kutler, P. and H. Lomax (1971, December). Shock-Capturing, Finite-Difference Approach to Supersonic Flows. Journal of Spacecraft and Rockets 8(12), 1175–1182.
[17]. Lorenzon, D. and S. Elaskar (2015). Simulacion de Flujos Supersonicos Bidimensionales y Axialmente Simetricos con OpenFOAM. Revista de la Facultad de Ciencias Exactas, Fisicas Y Naturales 2(2), 65–76.
[18]. Moretti, G. (1967). Analysis of Conical Flow on the Leeward Side of a Cone at Angle of Attack. General Applied Science Laboratories, Inc., Westbury, N.Y.
[19]. Rainbird, W. (1968a). The External Flow Field About Yawed Circular Cones. In AGARD Conference Proceedings, Volume 30.
[20]. Rainbird, W. (1968b, January). Turbulent boundary-layer growth and separation on a yawed cone. New York, NY, U.S.A. American Institute of Aeronautics and Astronautics.
[21]. Sims, J. (1964). Tables of Supersonic Flow Around Circular Cones at Small Angle of Attack. Technical Report NASA SP-3000.
[22]. Tamagno, J., S. Elaskar, and G. Rios Rodriguez (2003, December). Numerical simulation of time-dependent reacting flows in pulse facilities. Applied Numerical Mathematics 47(3- 4), 515–530.
[23]. Taylor, G. and J. Maccoll (1933a, February). The Air Pressure on a Cone Moving at High Speeds. I. Proceedings of the Royal Society A: Mathematical, Physical and Engineering Sciences 139(838), 278–297.
[24]. Taylor, G. and J. Maccoll (1933b, February). The Air Pressure on a Cone Moving at High Speeds. II. Proceedings of the Royal Society A: Mathematical, Physical and Engineering Sciences 139(838), 298–311.

[25]. Toro, E. (2009). Riemann Solvers and Numerical Methods for Fluid Dynamics. Berlin, Heidelberg: Springer Berlin Heidelberg.
[26]. Tracy, R. (1963). Hypersonic Flow over a Yawed Circular Cone.
[27]. Yahalom, R. (1971). An Experimental Investigation of Supersonic Flow Past Yawed Cones. Aeronautical Sciences Division, University of California, Berkeley, California.
[28]. Zang, B., V. Us, H. Lim, X. Wei, and T. New (2018, September). An assessment of OpenFOAM solver on RANS simulations of round supersonic free jets. Journal of Computational Science 28, 18–31.